

CONVERGENCE OF THE CRITICAL COOLING RATE FOR PROTOPLANETARY DISK FRAGMENTATION  
ACHIEVED; THE KEY ROLE OF NUMERICAL DISSIPATION OF ANGULAR MOMENTUM

HONGPING DENG,<sup>1</sup> LUCIO MAYER,<sup>1</sup> AND FARZANA MERU<sup>2</sup>

<sup>1</sup>*Center for Theoretical Astrophysics and Cosmology, Institute for Computational Science, University of Zurich, Winterthurerstrasse 190, 8057 Zurich, Switzerland*

<sup>2</sup>*Institute of Astronomy, University of Cambridge, Madingley Road, Cambridge, CB3 0HA, UK*

(Received July 1, 2016; Revised September 27, 2016; Accepted July 22, 2018)

Submitted to ApJ

ABSTRACT

We carry out simulations of gravitationally unstable disks using smoothed particle hydrodynamics (SPH) and the novel Lagrangian meshless finite mass (MFM) scheme in the GIZMO code (Hopkins 2015). Our aim is to understand the cause of the non-convergence of the cooling boundary for fragmentation reported in the literature. We run SPH simulations with two different artificial viscosity implementations, and compare them with MFM, which does not employ any artificial viscosity. With MFM we demonstrate convergence of the critical cooling time scale for fragmentation at  $\beta_{crit} \approx 3$ . Non-convergence persists in SPH codes, although it is significantly mitigated with schemes having reduced artificial viscosity such as inviscid SPH (ISPH) (Cullen & Dehnen 2010). We show how the non-convergence problem is caused by artificial fragmentation triggered by excessive dissipation of angular momentum in domains with large velocity derivatives. With increased resolution such domains become more prominent. Vorticity lags behind density due to numerical viscous dissipation in these regions, promoting collapse with longer cooling times. Such effect is shown to be dominant over the competing tendency of artificial viscosity to diminish with increasing resolution. When the initial conditions are first relaxed for several orbits, the flow is more regular, with lower shear and vorticity in non-axisymmetric regions, aiding convergence. Yet MFM is the only method that converges exactly. Our findings are of general interest as numerical dissipation via artificial viscosity or advection errors can also occur in grid-based codes. Indeed for the FARGO code values of  $\beta_{crit}$  significantly higher than our converged estimate have been reported in the literature. Finally, we discuss implications for giant planet formation via disk instability.

*Keywords:* Gravitational instability — accretion, accretion disks — fragmentation — numerical viscosity

## 1. INTRODUCTION

Massive rotating gas disks can become unstable due to their own self-gravity. Using linear perturbation theory applied to an axisymmetric, razor-thin disk, [Toomre \(1964\)](#) showed that the exponential growth of local density perturbations is controlled by the parameter

$$Q \equiv \frac{c_s \kappa}{\pi G \Sigma} \quad (1)$$

where  $c_s$  is the sound speed in the disk,  $\kappa$  is the epicyclic frequency, which equals the angular frequency  $\Omega$  for a Keplerian disk, and  $\Sigma$  is the mass surface density ( $G$  is the gravitational constant). When  $Q < Q_{crit} \approx 1$ , gravitational instability occurs locally, and a gas patch will undergo collapse as gravity overcomes both pressure gradients and shear induced by rotation.

In realistic finite-thickness disks subject to generic perturbations the character of the instability is global, whereby the disk first undergoes a phase of non-axisymmetric instability, namely develops a prominent spiral pattern, before becoming locally unstable to collapse ([Durisen et al. 2007](#)). Inside and across spiral arms fluid elements are subject to torques that lead to angular momentum transfer ([Cossins et al. 2009](#)). Angular momentum transfer is indeed a key feature of gravitational instability, and ultimately determines the evolution of the density field in other over-dense regions inside spiral arms ([Mayer et al. 2004](#); [Boley & Durisen 2010](#)). The other central aspect is that the spiral pattern causes shocks in the flow, releasing gravitational energy into heat, and eventually raising  $Q$  above the stability threshold. More specifically, whether or not  $Q$  will remain low enough for the instability to grow, and eventually lead to fragmentation, ultimately depends on the ability of the gas to release the heat via radiative cooling. [Gammie \(2001\)](#) proposed to parameterize the local cooling time scale  $t_{cool}$  as

$$\beta = t_{cool} \Omega \quad (2)$$

where

$$t_{cool} = u \left( \frac{du}{dt} \right)^{-1} \quad (3)$$

$u$  is the specific internal energy. He showed that when  $\beta < \beta_{crit} \approx 3$  fragmentation occurs in local shearing sheet simulations with a ratio of specific heats  $\gamma = 2$ . Physically this means cooling has to occur on a timescale comparable to the local orbital time, which can be easily understood as the spiral pattern that generates shock heating also evolves on the local orbital time. Using 3D SPH simulations, [Rice et al. \(2005\)](#) showed  $\beta_{crit} \approx 6 - 7$  for disks with  $\gamma = 5/3$ . A similar value of  $\beta_{crit}$  was also found by [Mayer et al. \(2005\)](#) using a different 3D

SPH code while comparing the evolution of isolated and binary protoplanetary disks. However, [Meru & Bate \(2011a\)](#) carried out similar SPH simulations to those in [Rice et al. \(2005\)](#) and found non-convergence of the critical cooling rate when the resolution of the simulations was increased. They found disks can fragment at a higher  $\beta_{crit}$  value in higher resolution simulations. [Meru & Bate \(2012\)](#) suggested that the non-convergent behaviour was caused by extra heating due to artificial viscosity occurring at low resolution. At higher resolution, less heating is generated through artificial viscosity and a lower critical cooling rate (i.e. a larger  $\beta$ ) is capable of balancing the combined heating by gravitational instability and artificial viscosity. Earlier on [Paardekooper et al. \(2011\)](#) had run 2D simulations with the grid-based code FARGO, showing that the non-convergence problem is not specific to SPH. By running a large set of simulations with both 3D SPH and the 2D grid-based code FARGO, [Meru & Bate \(2012\)](#) concluded that  $\beta_{crit}$  should converge to an asymptotic value  $\approx 20 - 30$ . This has important implications since it suggests fragmentation can occur even with relatively long cooling times, corresponding to almost an order of magnitude longer than the local orbital time. If clumps produced by fragmentation can later evolve into gas giant planets (see eg. [Helled et al. \(2014\)](#)), it follows that giant planet formation via disk instability is more common than previously thought.

[Paardekooper et al. \(2011\)](#) suggested that the non-convergence is at least partly due to the emergence of special locations in the disk, at the boundary between the turbulent and the laminar region, which appear when the disk is still adjusting towards a well developed gravito-turbulent state. In order to avoid this edge effect, [Paardekooper \(2012\)](#) carried out high resolution 2D local shearing sheet FARGO simulations, but found a similar increase of  $\beta_{crit}$  as resolution increased. Fragmentation also exhibited a stochastic nature in his simulations. However, recently [Klee et al. \(2017\)](#) performed a numerical study arguing that stochastic fragmentation is probably caused by oversteepening when performing slope limiting in grid-based codes. Moreover, [Young & Clarke \(2015\)](#) showed that the fragmentation boundary is strongly related to the gravitational softening in 2D simulations. When the softening is comparable to the resolution scale  $\beta_{crit}$  increases with resolution, while when the softening is comparable to the disk scale height,  $\beta_{crit}$  varies little. [Young & Clarke \(2015\)](#) also showed that clumps form from overdensities with length-scales  $\sim H$ . This is consistent with the earlier result of [Gammie \(2001\)](#), who found no power at scales much smaller than  $H$ , which were resolved in the simula-

tions. These results combined suggest that, whatever is the nature of non-convergence, it should involve physics and/or numerics acting on a scale of order  $H$ .

In this paper, we attempt to explore again the issue of non-convergence by comparing different Lagrangian hydro methods which have by design different numerical dissipation. We are driven by the notion that non-convergence might be caused by numerical errors, perhaps associated with the boundary regions identified by Paardekooper et al. (2011). Our aim is to identify the exact source of non-convergence as well as a way to overcome the problem, in order to place self-gravitating disk simulations on a firm ground.

We run simulations using exactly the same initial condition of Meru & Bate (2012) with three different Lagrangian hydro methods. Specifically, we use the vanilla SPH implementation in the GIZMO code (Hopkins 2015), which is equivalent to the original GADGET3 code ((Springel 2005) with standard Monaghan artificial viscosity and Balsara switch (Balsara 1995), a modified version of the same code where we implemented the artificial viscosity scheme of Cullen & Dehnen (2010) (inviscid SPH, hereafter ISPH), and the new Lagrangian meshless finite mass(MFM) method in GIZMO (Hopkins 2015), which does not need any artificial viscosity. Finally, a smaller set of additional simulations exploring recent variants of the SPH method are presented at the end of the paper.

In section 2, we describe the setup of the simulations. In section 3, we present the main results. We discuss the interpretation and implications of our results in section 4, and finally draw our conclusions in section 5. Results of ancillary numerical tests are also presented in Appendix A and Appendix B.

## 2. SIMULATIONS

In order to compare with previous work, we use the same disk model as in Meru & Bate (2012). A  $0.1M_{\odot}$  disk spans a radial range,  $0.25 < R < 25$  AU, surrounding a solar mass star. The initial surface mass density and temperature profiles are  $\Sigma \propto R^{-1}$  and  $T \propto R^{-1/2}$ , respectively. The temperature is normalized so that at the outer edge of the disk the Toomre  $Q$  parameter equals 2. We use an adiabatic gas equation of state with  $\gamma = 5/3$ . We note that the problem is essentially scale free and we 1 solar mass, 1 AU, and 1yr as the mass, length and time unit respectively in our calculation. The simulations are run with different cooling rates as well as three different resolutions. The low resolution model (LR) comprises 250,000 particles, while 2 million and 16 million particles are used, respectively, in the high resolution (HR) and ultra-high resolution model(UHR). The

central star is modeled with a sink particle with sink radius of 0.25 AU. Gas particles reaching the sink radius are deleted and their mass and momentum are added to it to ensure mass and momentum conservation. We use adaptive gravitational softening(Price & Monaghan 2007).

The three disk models are run with the three different hydro-methods, namely standard vanilla SPH as in Meru & Bate (2012) (hereafter TSPH), inviscid SPH (ISPH), which uses the implementation of artificial viscosity by Cullen & Dehnen (Cullen & Dehnen 2010), and the MFM method. The first two methods differ only in the way artificial viscosity is implemented. In vanilla SPH we solve the fluid equations using the standard density-entropy formulation(Springel 2005) and standard Monaghan artificial viscosity with Balsara switch (Balsara 1995), designed to reduce viscosity in flows with high vorticity. In ISPH we use the same formulation of the hydro equations but we use the Cullen & Dehnen viscosity which uses the time derivative of the velocity divergence as shock indicator in order to eliminate numerical viscous dissipation away from shocks. In this formulation, particles have individual adjustable viscosity coefficients between an  $\alpha_{max}$  and an  $\alpha_{min}$  value, and are further assigned a coefficient  $l$  that sets the decay time of viscosity away from shocks. Therefore the latter formulation requires to set three parameters instead of the conventional two coefficients  $\alpha_{sph}$  and  $\beta_{sph}$  in the standard Monaghan viscosity. While previous artificial viscosity schemes had appeared that used switches acting on individual particles Morris & Monaghan (1997), including with similar parameterization (Rosswog et al. 2000), the ISPH method is a further improvement towards a truly inviscid method owing to its shock tracking procedure. The MFM method is instead an entirely different method to solve the hydrodynamical equations, but shares with SPH the Lagrangian approach and the use of particles as tracers of the fluid. Most importantly, it does not need any artificial viscosity in order to generate stable solutions, even in high Mach number flows, hence it is by nature inviscid. While we defer the reader to Hopkins (2015) for a detailed description of the code here we recall that MFM uses the SPH-like kernel of a particle distribution to construct a volume partition of the domain. The fluid equations are then solved on the unstructured mesh thus generated by the partition using a Riemann solver (HLLC in this paper, see Hopkins (2015)). As the volume elements are constructed from the particles the smoothing length  $h$  of the assigned kernel function still defines the fundamental resolution length as in SPH. The method conserves mass, momentum and angular momentum by design as an SPH code,

but this is even more strictly true for angular momentum relative to SPH since there is no added artificial viscosity, as pointed out and demonstrated with a series of tests in Hopkins (2015). Being an integral formulation, in this sense a hybrid with finite-volume grid-based methods, it should also not suffer from the errors associated with poor estimates of gradients proper of SPH. Gravity is solved using the same tree code in all three methods, inherited from the progenitor GADGET3 code.

For all codes we employ two different techniques to start the simulations. In the first one we start directly from the initial disk model without any relaxation phase, while in the second one we first relax the system by running the disk for 4 outer rotation periods (ORPs) with relatively long cooling time, using  $\beta = 12$ . By relaxing the initial condition in the second case we allow the development of a gravoturbulent state, with sustained spiral structure but no fragmentation, and then switch to the desired  $\beta$  value. The latter setup, which we indicate with TIC (turbulent initial condition) resembles that adopted by Paardekooper et al. (2011). It avoids the transition from a smooth disk to a turbulent disk as in figure 3. We will show this transition can lead to numerical fragmentation, as also found by Paardekooper et al. (2011). For both initial setups, once the desired cooling timescale is turned on, simulations are run either for at least 6 ORPs, or until the disk fragments.

In order to facilitate comparisons we adopt standard values of artificial viscosity parameters in both TSPH and ISPH runs. For TSPH runs we use the Monaghan viscosity with  $\alpha_{sph} = 1$  and  $\beta_{sph} = 2$ , which is the default choice for flows in which high Mach numbers can arise (Hernquist & Katz 1989), and has been advocated also by Mayer et al. (2004) and Meru & Bate (2012). For ISPH we set  $\alpha_{max} = 2$ ,  $\alpha_{min} = 0$  and  $l = 0.05$  (Cullen & Dehnen 2010).

We declare a disk to undergo fragmentation (labeled ‘‘F’’ in table 1) when clumps form that are at least two orders of magnitude denser than their surroundings and can survive at least one outer rotation period without being sheared apart. Transient overdensities can form in the runs that we label ‘‘NF’’ but no robust clumps form in the way just defined. The results of simulations are summarized in Table 1, where we indicate whether or not the disk fragments, and for which value of  $\beta$ .

### 3. RESULTS

#### 3.1. Overview

Table 1 summarizes our results on fragmentation. It highlights three main results borne out of our suite of runs. First, the TSPH runs confirm the dependence

**Table 1.** Simulations fragmented are marked with F, otherwise are marked with NF. The boundary between fragmentation and non-fragmentation is marked with green color.

| Simulation  | $\beta =$ |     |    |    |    |    | Boundary |
|-------------|-----------|-----|----|----|----|----|----------|
|             | 3         | 3.5 | 4  | 5  | 6  | 8  |          |
| TSPH-LR     |           |     |    | F  | F  | NF | 6-8      |
| ISPH-LR     |           |     |    | F  | NF |    | 5-6      |
| MFM-LR      | F         | F   | NF | NF |    |    | 3.5-4    |
| TSPH-HR     |           |     |    |    |    | F  | >8       |
| ISPH-HR     |           |     |    |    | F  | NF | 6-8      |
| MFM-HR      | F         | F   | F  |    | NF | NF | 4-6      |
| TSPH-LR-TIC |           | F   | NF |    |    |    | 3.5-4    |
| TSPH-HR-TIC |           |     | F  | NF |    |    | 4-5      |
| MFM-LR-TIC  | F         | NF  |    |    |    |    | 3-3.5    |
| MFM-HR-TIC  | F         | NF  |    |    |    |    | 3-3.5    |
| MFM-UHR-TIC | F         | NF  |    |    |    |    | 3-3.5    |

of the critical  $\beta$  for fragmentation on resolution. Second, we can infer that non-convergence with resolution is strongly mitigated by methods that reduce numerical dissipation in shear flows. This includes improved SPH artificial viscosity schemes designed to reduce it in shear flows, as in the case of ISPH, but is even more evident for a new hydro schemes with no explicit numerical viscosity, such as MFM. Third, *exact* convergence is obtained only with MFM but demands the to start from a relaxed, gravoturbulent initial setup, confirming the claim of Paardekooper et al. (2011) (see Table 1, ‘‘TIC’’ runs). Without relaxation a marginal increase of the critical  $\beta$  with increasing resolution persists. In section 3.2 we will provide an explanation of these main findings.

At low resolution the fragmentation boundary in TSPH is found to lie between  $\beta = 6$  and  $\beta = 8$ , which is slightly higher than the fragmentation boundary  $\beta = 5.5 - 5.6$  in Meru & Bate (2011a). However, in their default setup Meru & Bate (2011a) use  $\alpha_{sph} = 0.1$  and  $\beta_{sph} = 0.2$ . If we compare instead with the subset of their runs that adopted  $\alpha_{sph} = 1$  and  $\beta = 2$ , consistent with ours, our results are in substantial agreement. Note that Meru & Bate (2012) show that using low values of the coefficients  $\alpha_{sph}$  and  $\beta_{sph}$  can result, counterintuitively, in high dissipation resulting from random particle motion. The noisier shear flow resulting in SPH simulations with lowered coefficients in the standard



Monaghan viscosity scheme had previously been shown to enhance fragmentation in locally isothermal simulations (Mayer et al. 2004). We also remind the reader that  $\alpha_{sph} = 1$  and  $\beta = 2$  are the preferred values for high Mach number flows in a variety of astrophysical regimes, and have been advocated for both galactic and protoplanetary disk simulations (Mayer et al. (2004); Kaufmann et al. (2007)).

Figure 1 shows runs using the three hydro implementations for  $\beta$  values near critical. The markedly different behaviours at equivalent high resolution is evident. MFM needs  $\beta = 4$  or lower to fragment, depending on the initial conditions setup, while TSPH fragments for a  $\beta$  twice as large, and ISPH falls in between. We remind the reader that between TSPH and ISPH the only difference is the implementation of artificial viscosity.

The Figure also shows how MFM simulations starting from turbulent initial conditions (TIC) are resilient to fragmentation even with very fast cooling at the highest resolution (UHR, see bottom right panel). The TIC simulations also exhibit a more flocculent spiral pattern dominated by lower order modes relative to the non-relaxed simulations, and this is true for all codes.

### 3.2. Numerical dissipation in MFM runs

When comparing TSPH and ISPH with MFM differences in the hydro implementation are more subtle. Indeed MFM does not have explicit numerical viscosity, rather it solves the hydro equations analogously to a finite volume method using a Riemann solver on volume elements mapped from the particle distribution. There could be some residual numerical dissipation associated with the non-analytical Riemann problem solution, but at the same time MFM does not advect fluid elements through a grid, a common source of numerical dissipation in finite volume grid-based methods. In the Keplerian ring test shown in Hopkins (2015) MFM conserves angular momentum better than all the other methods it was compared to, including SPH with a modified hydro force (pressure-entropy, hereafter PSPH) that helps to remove unwanted numerical effects, such as artificial tension, at fluid interfaces. This would suggest MFM is inherently less viscous than all variants of SPH, irrespective of the artificial viscosity scheme adopted. However in the latter test the disk is 2D, adiabatic and non self-gravitating, which is very different from the configuration we are studying here. Therefore, in order to reassess that MFM is indeed less viscous in a relevant albeit simple configuration we run two different test problems. First we consider the rotating uniform isothermal sphere collapse test in Boss & Bodenheimer (1979). The results are shown in appendix A. We find that an-

gular momentum is transported slightly faster outwards in TSPH runs as expected from stronger numerical viscous transport, albeit differences are small and overall the angular momentum profiles are comparable between the two codes at late times. Furthermore, in appendix B, we use an *accreting* sink particle in a shearing sheet configuration. Here the flow responds more abruptly to the strong gravitational pull of the sink, and differences between the three methods emerge more clearly, establishing that MFM has better angular momentum conservation in flows with large velocity gradients. While we find that ISPH, as expected, has a lower numerical viscosity, the accretion rate, as measured by the growth of the central density, is comparable to TSPH. Instead, MFM leads to consistently smaller density increase, and the differences remains over time.

In addition to angular momentum dissipation, the evolution of the internal energy is another important proxy for how strong the numerical dissipation by artificial viscosity is, especially in spiral shocks. Figure 2 shows the internal energy measured at the disk mid-plane after 1.07 ORPs in a non-fragmenting hi-res run (for which we used a large enough  $\beta = 8$  to avoid fragmentation). A non-fragmenting run is a conservative choice for our purpose since spiral shocks are weaker. The Figure highlights how the MFM run exhibits the cooler profile everywhere because, at an equivalent cooling rate, it suffers less from artificial viscous heating, even in the region near the inner boundary where SPH is notoriously problematic in handling the rapidly increasing shear (Mayer et al. 2004; Kaufmann et al. 2007). The TSPH and ISPH simulations are almost indistinguishable. The similar internal energy peak occurs slightly above 20 AU in all runs because that is where a strong ring-like overdensity develops (similar to those in the upper panel of Figure 3), suggesting that where the flow is intrinsically more compressive in all codes the dominant heating comes from PdV work rather than numerical viscosity.

Having now assessed that MFM is the less viscous among the methods considered, we can turn again to the interpretation of the results in Figure 1. If, as suggested in Meru & Bate (2012), reduced numerical viscous heating as the resolution is increased is the source of non-convergence, one would expect that MFM runs should be more prone rather than less prone to fragmentation relative to TSPH and ISPH runs. This is because gas can cool more effectively at a given  $\beta$ , as we have just seen by comparing the internal energy evolution. Instead the opposite trend is seen – MFM is less prone to fragmentation and its behaviour is nearly convergent with resolution (exactly convergent in TIC runs). Furthermore, ISPH and TSPH appear to be

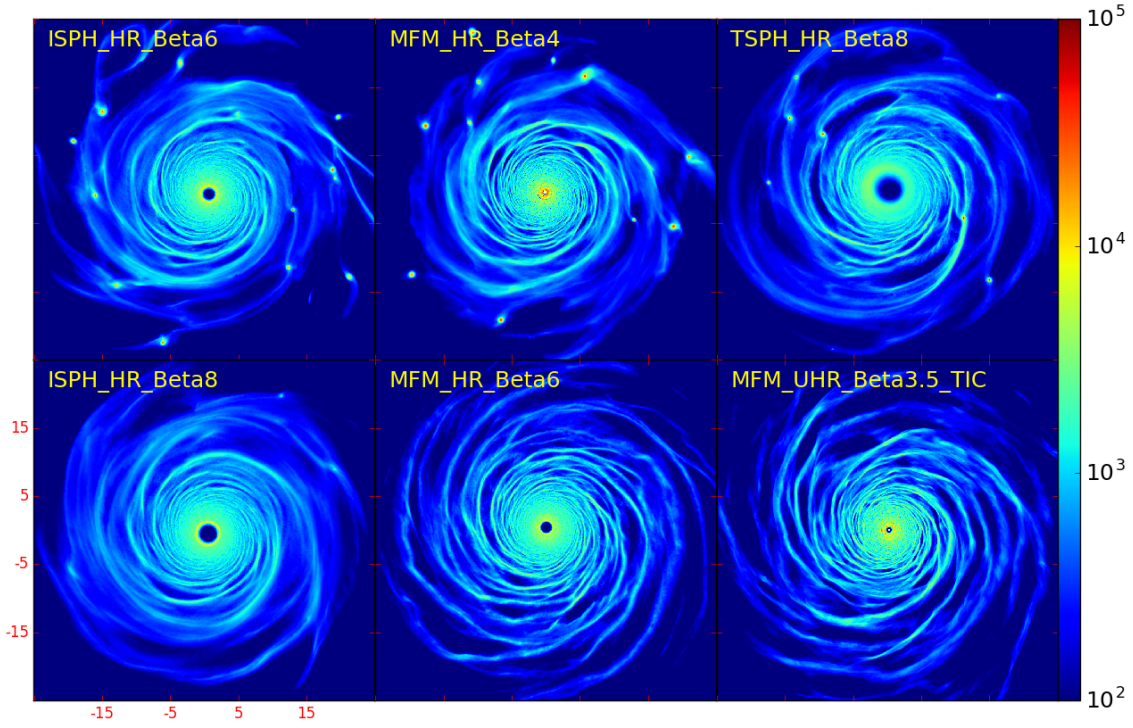


**Figure 1.** Surface mass density ( $[g/cm^2]$ ) in logarithmic scale. The box size is 50 code units (axes in code units are shown in red at the bottom left corner). A subset of the simulations for the three different methods and with  $\beta$  near critical is shown to highlight that MFM and ISPH do not fragment with much lower values of  $\beta$  relative to TSPH at comparable resolution (compare bottom panel to top panel). A TIC run at even higher resolution (UHR) is also shown in the bottom right panel, which also does not fragment despite a very low  $\beta$  (see Table 1). From the first to the second row, left to right, snapshots are taken at 3.7, 0.8, 5.8, 6, 6, 6 ORPs. Note the different times were chosen for the snapshots in the top panel according to when fragmentation begins, which is much earlier than the time chosen in the bottom panel. The non-fragmenting runs have reached a self-regulated state even before 6ORPs, which is thus a reliable reference time.

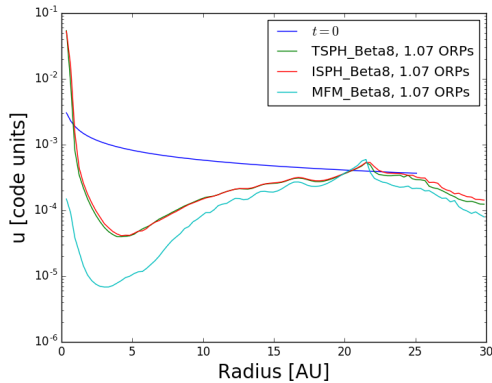


**Figure 2.** Azimuthally averaged radial internal energy profile in the disk mid-plane, in code units and logarithmic scale at 1.07 ORPs. The HR simulations run with different hydro methods are shown. The MFM run has a much cooler disk due to less numerical viscosity and thus reduced numerical heating (see Section 3).

equivalent when we inspect the internal energy evolution

in Figure 2, yet ISPH is less prone to fragmentation. All this suggests that, in order to understand the nature of our results, among the effects associated with numerical viscous dissipation, enhanced angular momentum transport, as opposed to enhanced heating, is key. We discuss this crucial point, as well as dependence on resolution, in the next section.

### 3.3. Numerical dissipation and the resolution-dependent flow properties

In standard SPH methods artificial viscosity is needed for the stability of the flow near discontinuities. Without that particle-interpenetration occurs and shocks cannot be properly resolved. The conventional form of artificial viscosity employs two terms (Monaghan & Gingold 1983; Springel 2005); one term linear in the divergence of the flow, controlled by the  $\alpha_{sph}$  coefficient, and one term with quadratic dependence on the flow divergence, controlled by  $\beta_{sph}$ . The quadratic term is dominant in shocks. When  $\beta_{sph} = 0$ , the linear term can be re-

cast in a shear viscosity  $\eta = (1/2)\alpha_{sph}\kappa hc_s\rho$  and a bulk viscosity  $\zeta = (5/3)\eta$ , where  $h$  is the SPH smoothing length, which controls the resolution, and  $\kappa$  is a constant that should be chosen according to the kernel (Cullen & Dehnen 2010). The shear component of the viscosity will always be present, namely also in non-shocking regions, and can generate artificial angular momentum transport in shearing flows such as those inherent to astrophysical disks, even in presence of damping factors dependent on the local vorticity such as the Balsara switch (Kaufmann et al. 2007). Cullen & Dehnen (2010), building on previous work (Morris & Monaghan 1997; Rosswog et al. 2000) proposed a new artificial viscosity switch with a high order shock indicator which results, in a much more effective damping of shear viscosity away from shocks. It is thus expected that, at fixed resolution, ISPH runs, which employ the latter viscosity scheme, should be less affected by numerical dissipation of angular momentum. At the same time, we caution that one expects mild shocks to arise as the spiral pattern grows in amplitude and the disk becomes marginally unstable, which could then result in significant viscous dissipation even in ISPH.

Having shown in more than one way, in the previous section, that MFM is a less viscous method, and knowing that ISPH is by construction less viscous than TSPH, we have inferred that the different susceptibility to fragmentation of the three type of runs must be somehow caused by the different degree of angular momentum dissipation. The next step is to address how angular momentum dissipation affects fragmentation. Moreover, there is a related puzzling fact emerging from Table 1. This is that one would expect the results of hydro methods whose main difference is the viscous dissipation of angular momentum should eventually converge as the resolution is increased because, owing to the dependence of shear viscosity on the smoothing length  $h$  just highlighted, viscous dissipation should decrease as resolution increases. Instead the opposite is seen;  $\beta_{crit}$  keeps increasing for TSPH as the resolution is increased, hence departing more and more from the  $\beta_{crit}$  value determined with MFM. However, we caution already at this point that this conventional way of reasoning is correct only if no other property of the flow changes with increasing resolution. If, for some reason, velocity gradients become intrinsically stronger as resolution is increased, as one could imagine that convergence might be hard to achieve irrespective of resolution.

Here we argue that the *nature of the flow in gravitationally unstable disks does change as resolution is increased*. It develops regions of stronger shear and vorticity as sharper flow features become resolved, and such

regions then become sites of higher numerical viscous dissipation. The resolution-dependent nature of the flow also explains why the way the initial setup is prepared matters for the fragmentation outcome *at varying resolution*, as we illustrate below. The changing nature of the flow with resolution is well illustrated in figure 3. The simulations using unrelaxed initial conditions offer the best tool to understand what happens. In these the spiral pattern originates in the inner disk and propagates outwards (Meru & Bate 2011b). We refer to the stage before spirals reach the outer edge of the disk as the *transition phase*. The duration of such transition phase depends on the cooling rate, but in general lasts about 2 ORPs. By visual inspection it is clear that at higher resolution non-axisymmetric modes are better resolved. This is the result of an improved gravitational force resolution, a point already emphasized in Mayer et al. (2004), Mayer & Gawryszczak (2008) for both SPH and adaptive mesh refinement (AMR) codes.

We refer to the boundary zones between the turbulent, highly non-axisymmetric flow component generated by gravitational instability and the background smooth, axisymmetric disk as the *interface region*. As seen in the upper panels of figure 3, these are regions roughly a few code units in size, and occur during the transition phase (see the rectangular region in Figure 3). Afterwards the entire disk becomes non-axisymmetric and gravito-turbulent. These interface regions are relevant because they are the location of the largest local velocity gradients, associated with both strong shear and vorticity.

We will use the analysis of vorticity as a proxy for high velocity derivatives in the flow as vorticity also carries information on the local angular momentum, which we posit plays a central role. The azimuthally averaged vorticity profile in the mid-plane is plotted in figure 4 for MFM runs at different resolution. In all of them it is evident that vorticity can be an order of magnitude higher than the Keplerian flow vorticity. These vorticity peaks occur near interface regions and more pronounced and more frequent as resolution increases. The latter is an effect of increased force resolution as higher overdensities appear that induce higher local vorticity. Indeed, if numerical dissipation of angular momentum does not affect the properties of the flow one would expect density and vorticity to remain correlated. Let us consider an approximately spherical *cusp* of the flow located at the interface, namely an overdense region of radius  $R_c$  and enclosed  $M_c$ , so that its mean density is  $\rho = M_c/R_c^3$ . When the cusp density is large enough a fluid element at its boundary will move with a (circular) velocity  $V_c$  such that  $\sqrt{G\rho} \propto \frac{V_c}{R_c}$ . In other words, the cusp dominates

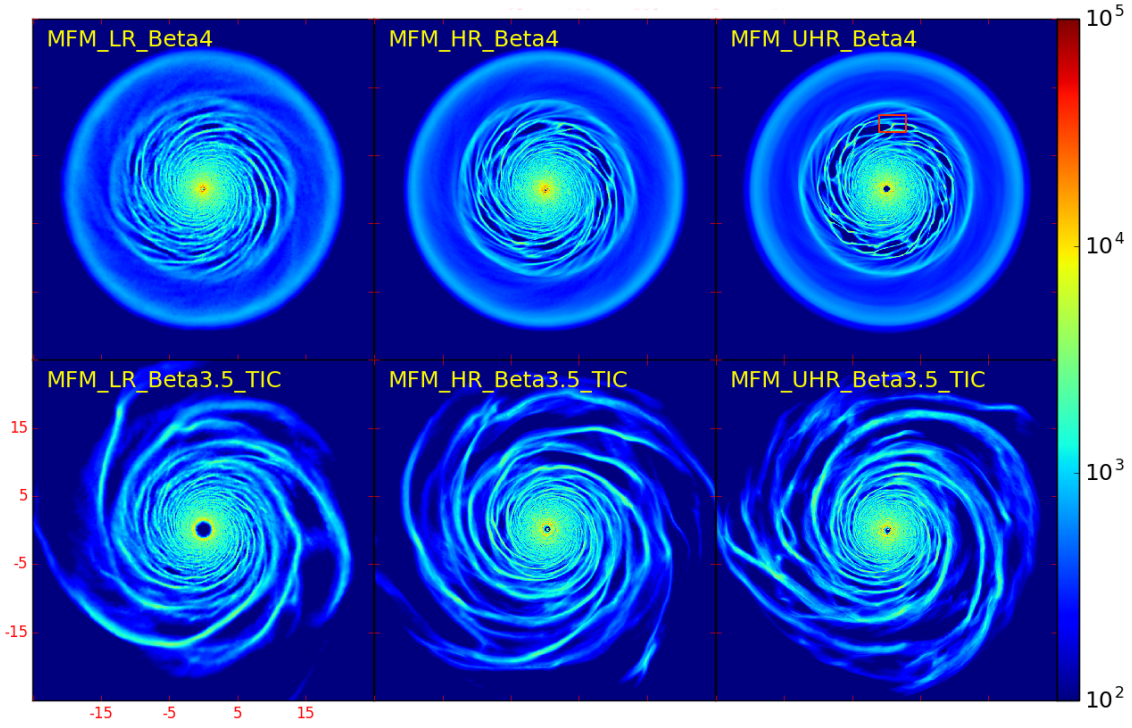


**Figure 3.** Surface mass density ( $[g/cm^2]$ ) in logarithmic scale for a subset of the MFM simulations run with different resolution and  $\beta$  close to critical (axes in code length units are shown in red at the bottom left corner). The bottom panel shows the TIC runs. Resolution increases by nearly 3 orders of magnitude from left to right. All snapshots are taken at 1.07 ORPs. A cusp is highlighted in the red box in the top right panel. Cusps form in the interface regions between spirals and outer smooth flow. They cause strong numerical dissipation and are absent in TIC runs (compare bottom and top panels).

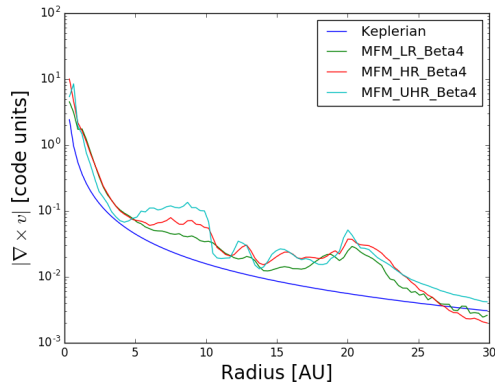


**Figure 4.** Azimuthally averaged radial vorticity profile in the disk mid-plane (the modulus of vorticity is in code units) measured at 1.07 ORPs for MFM simulations with different resolution. The vorticity of a pure Keplerian flow is also shown for comparison

the local gravitational field, even if collapse has not ensued, so that locally the vorticity of the flow should be correlated with local density, since, dimensionally, the vorticity  $\nabla \times \mathbf{v} \propto \frac{V_c}{R_c} \sim \sqrt{G\rho}$  ( $\mathbf{v}$  is the velocity vector

of the gas flow) We can now turn back to our simulations and check whether or not vorticity and density in the cuspy regions grow at the relative rates implied by the proportionality just highlighted. First of all, we notice that the peak density at interface regions in MFM runs in Figure 3 is almost an order of magnitude larger in the UHR simulation relative to the LR simulation. As expected, vorticity is correspondingly higher (Figure 5). Note that TSPH runs share the same trend. ISPH runs yield a similar vorticity map as TSPH because at interface regions the flow has high velocity derivatives hence artificial viscosity is not suppressed by the Cullen & Dehnen switch.

We cannot compare the vorticity in the MFM and SPH simulations in figure 5 directly because the disk is much cooler in MFM (see figure 2) so that the spiral pattern evolves faster than in the SPH simulations. But we can still compare the evolution of maximum density and maximum vorticity in a relative sense. We focus on the transition phase of a set of fast cooling simulations with  $\beta = 4$ . We plot the peak volume density and peak vorticity in the  $r > 8$  region in figure 6. At  $t = 2$  ORPs the spiral pattern reaches the outer edge



of the disk in all simulations. In SPH simulations very compact, dense clumps have formed at this point while in MFM only loosely bound overdensities are present. The peak density in MFM is indeed lower than in SPH simulations at comparable resolution. Also, SPH simulations show an exponential growth of the peak density which is absent in the MFM simulation. The figure also shows that, in the early stage of the transition phase, the MFM run experiences a faster growth of density perturbations, reflecting the lower temperature (see Figure 2). Yet the key result emerges when we compare density and vorticity evolution in the different runs. It is noteworthy that in MFM runs vorticity appears to grow at the rate expected based on the relation  $\nabla \times \mathbf{v} \propto \sqrt{G\rho}$ . Indeed at 2 code units it has grown by about an order of magnitude while density has grown by nearly two orders of magnitude. Conversely, a comparable increase in vorticity occurs in TSPH and ISPH runs at this time but there density increases much more, by about four orders of magnitude. We argue that this remarkable mismatch reflects strong numerical dissipation of angular momentum near cusps, which damps vorticity and promotes collapse.

We can attempt to understand the nature of the problem by considering resolution requirements in self-gravitating disks. In order to properly follow the fragmentation, the most unstable Toomre wavelength  $\lambda_T$  must be resolved (Nelson 2006). This is

$$\lambda_T = \frac{2c_s^2}{G\Sigma} \quad (4)$$

where  $\Sigma \sim \rho H$  and in a marginally unstable disk, ( $\Sigma$  and  $H$  are, respectively, surface density and disk scale height). Note that the most unstable wave number  $\frac{2\pi}{\lambda_T}$  is exactly the inverse of the disk thickness, so that, dropping constant factors we can write  $\lambda_T \sim Q \frac{c_s}{\Omega} \sim H$  (Cossins et al. 2009). Since  $Q \sim 1$  when the disk becomes unstable, for a Keplerian disk, we substitute  $\Sigma$  with  $\rho\lambda_T$  in equation 4. We can then write  $\lambda_T \sim \frac{c_s}{\sqrt{G\rho}}$ . We recall that the Toomre wavelength is borne out of linear perturbation theory for axisymmetric local perturbations. It is a conservative resolution marker for our purpose since it has been shown that the nonlinear stage of fragmentation in spiral arms occurs on a characteristic wavelength that is 5-6 times smaller than the Toomre wavelength (Boley 2009; Tamburello et al. 2015). In the interface regions the spiral pattern dominates the flow hence the same considerations would apply. Recalling again that, near cusps, we can write  $\sqrt{G\rho} \propto \frac{V_c}{R_c}$  and  $\frac{V_c}{R_c} \sim \nabla \times \mathbf{v}$ , we obtain:

$$\frac{\lambda_T}{h} \sim \frac{c_s}{h|\nabla \times \mathbf{v}|} \quad (5)$$

We define

$$q \equiv \frac{c_s}{h|\nabla \times \mathbf{v}|} \quad (6)$$

where  $h$  is the kernel smoothing length. Since the Toomre wavelength should be resolved by at least one kernel (Nelson 2006), the resolution will not be adequate if  $q < 1$  bearing in mind that the Toomre wavelength is a generous estimate for the characteristic wavelength of fragmentation. Likewise, the equation above highlights how, as vorticity increases, the resolution has to increase proportionally, namely the smoothing length  $h$  has to decrease, in order to maintain  $q$  large and thus follow a self-gravitating fluid appropriately. The upper panel of Figure 7 shows that, as we expected,  $q < 1$  in the interface regions, and decreases as resolution is increased, reflecting the dominant effect of increasing vorticity relative to the smoothing length decrease.

Conversely, outside these regions  $q$  increases as resolution is increased, as the dominant effect is now the decrease of the smoothing length. Note that Figure 7 uses the MFM runs. The lower panel of Figure 7 also shows that  $q$  is always high *at all resolutions* when the initial conditions are relaxed (TIC runs), which reflects the fact that, even for MFM, only in this case there is exact convergence for the critical cooling time (see Table 1).

Indeed in TIC runs the velocity field of the flow varies more smoothly across the disk, with no transition phase and thus no cusps (Figure 3). This confirms the claim of (Paardekooper et al. 2011) on the importance of the initial setup for convergence studies. This is because artificial angular momentum transport during the transition from a smooth disk to a fully developed spiral pattern is avoided. Yet table 1 also shows that only MFM shows exact convergence among TIC runs ( $\beta_{crit} = 3$ ). The SPH runs still have excessive viscous dissipation of angular momentum even in presence of more moderate velocity gradients in shearing flows. While we did not run ISPH with TIC conditions, we have already shown that the viscosity switch alone becomes rather ineffective at high resolution, resulting in a behaviour similar to TSPH (Figure 6).

#### 4. DISCUSSION

Fragmentation in self-gravitating disks is known to be a process highly sensitive to the numerical implementation of the hydrodynamical equations and resolution. Earlier work carried out with both grid-based and SPH codes highlighted the importance of numerical approaches, including the effect of artificial viscosity, for the simple case of locally isothermal disks (Pickett et al. 2001; Mayer et al. 2004; Durisen et al. 2007; Mayer & Gawryszczak 2008). Strong dependence on numerics has also been seen in cloud fragmentation simulations.

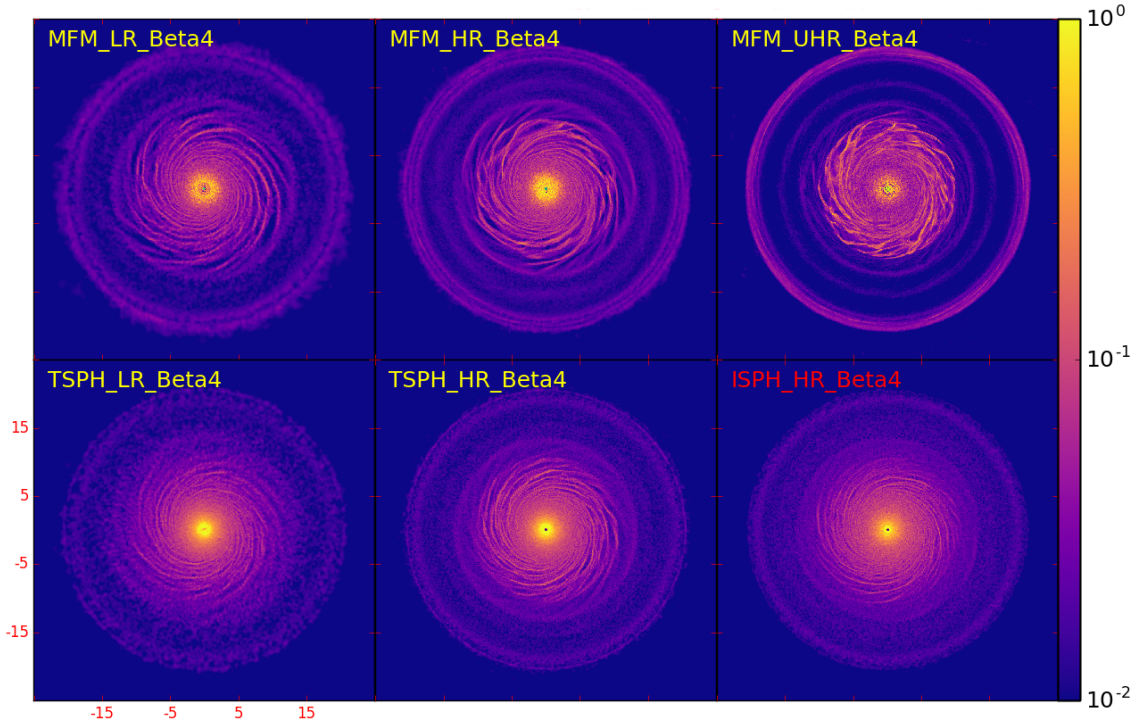


**Figure 5.** Vorticity maps. We show the modulus of vorticity in the disk mid-plane, in code units (axes in code length units are shown in red at the bottom left corner). In the innermost regions, vorticity is dominated by the Keplerian rotation, see the vorticity profile in figure 4. In the MFM simulations (top row), as the resolution increases the vorticity due to local overdense regions increases, as such regions become better resolved and are characterized by strong departures from the background flow velocity. The corresponding peak volume density in code units, in the interface region (located at 8-11 code length units), from left to right, upper to lower, is 0.0026, 0.0081, 0.019, 0.0013, 0.0048, 0.0031.

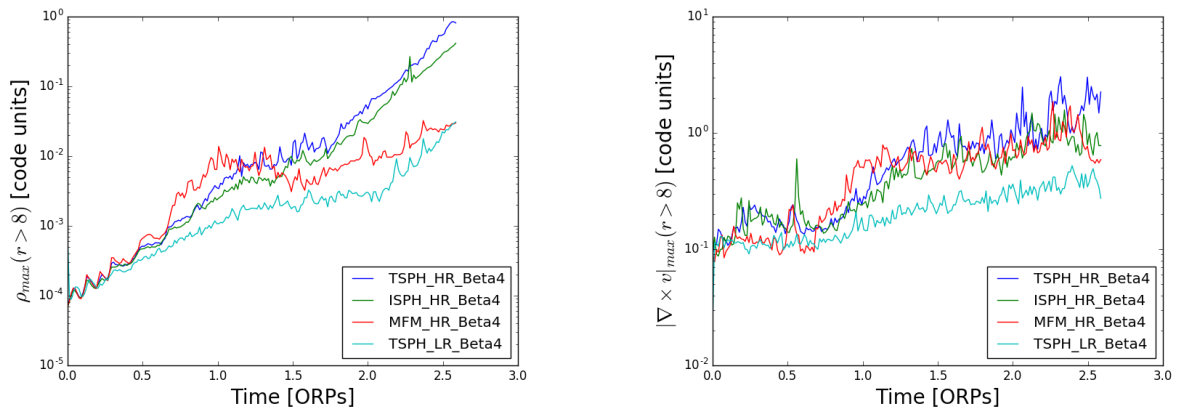


**Figure 6.** Peak volume density (left) and peak vorticity (right) at  $r > 8$ , which includes the interface region, in the first 2.7 ORPs. We show results for TSPH, ISPH and MFM runs at different resolutions. The peak density of SPH simulations grows exponentially after the spirals reach the outer edge of the disk at about 2 ORPs. The peak vorticity is uncorrelated with the peak density, see discussion in section 3

For example, [Bate \(2011\)](#) carried out SPH simulations of molecular cloud collapse to form protostars and disks, and found more fragmentation with increasing resolu-

tion. [Hu et al. \(2014\)](#) ran galaxy simulations with the SPH code GADGET ([Springel 2005](#)) and showed differ-

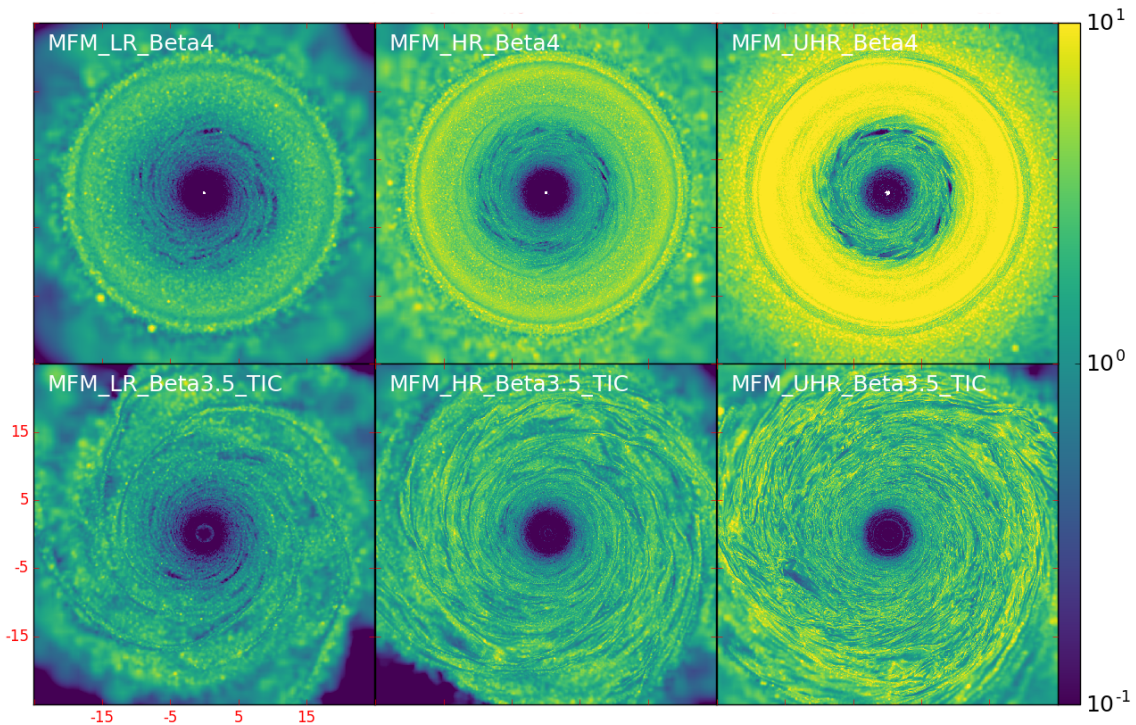


**Figure 7.** The  $q$  factor at 1.07 ORPs in MFM runs at different resolution. The top panel shows the standard runs, while the bottom panel shows the TIC runs. As the resolution increases  $q$  increases mainly because of a smaller smooth length. However, in the interface regions, especially between spirals,  $q$  can become very small which indicates strong numerical dissipation (see dark spots, even more prominent at higher resolution in the top panel). These regions are not present in the TIC runs, where correspondingly  $q$  is higher on average and increases with increasing resolution everywhere, in sharp contrast with the runs in the top panel. The innermost regions have small  $q$  due to strong background shear but are Toomre stable and axisymmetric so our arguments in Section 3 do not apply.

ent artificial viscosity switches can lead to very different fragmentation results.

In this paper we have shown that simply increasing the resolution does not yield a more correct answer for disk fragmentation, rather the nature of viscous dissipation and how it couples with the properties of the flow is the crucial aspect. Since the properties of the flow change with resolution, studying convergence as a function of resolution alone is insufficient, Instead comparing different hydro methods, and in particular different methods with varying numerical dissipation, reveals the real nature of the problem. Angular momentum dissipation in strong shearing regions, which we study using vorticity, is the main reason behind non-convergence in SPH methods. ISPH, which suppresses artificial viscosity in pure shearing flows, improves considerably but does not fully converge, likely because in regions of high vorticity the flow is also highly compressive so that viscosity turns on based on the shock tracking scheme.

MFM is the only method for which we were able to prove convergence of the critical cooling timescale

among the methods explored so far, but even in this case exact convergence requires relaxation of the initial conditions in order to avoid transients that lead to sharp flow velocity gradients and high local vorticity at interface regions. The important role of the initial conditions is supported also by a recent study of [Backus & Quinn \(2016\)](#) with locally isothermal disks using a modern formulation of the SPH hydro force, but still standard artificial viscosity, using the ChaNGa code. It is also in line with previous findings by [Paardekooper et al. \(2011\)](#) with the FARGO code.

Clearly we have only considered a small set of hydro methods in this paper. Even in the context of SPH many different revised formulations of the hydro force have appeared in the literature over last few years which would be worth exploring, such as SPHS ([Hayfield et al. 2011](#)), GDSPH ([Keller et al. 2014](#); [Tamburello et al. 2015](#)) and the, pressure-entropy formulation (PSPH) in [Hopkins \(2013\)](#). Thermal diffusion alone has been shown to be effective at removing artificial surface tension ([Price 2008](#); [Shen et al. 2010](#)). It may play a role as it does in all



problems where sharp fluid interfaces appears (Agertz et al. 2007). These modifications of other aspects of the SPH formulation could also affect  $\beta_{crit}$ . The smoothed cooling approach of Rice et al. (2014) is also another example of how the fragmentation problem is sensitive to the details of the numerical implementation within the same category of methods. In order to at least partially address this we rerun the HR simulation from relaxed initial conditions (TIC) using PSPH and thermal diffusion in the GIZMO code (Hopkins 2015), and with the Cullen & Dehnen viscosity formulation. We find that the disk fragments for  $\beta = 4 - 5$ . Therefore using PSPH does not lead to an improvement relative to SPH, confirming the central role of residual viscous dissipation as opposed to other aspects of the SPH scheme, for example the SPH “E0” zeroth-order errors (Read et al. 2010).

Dehnen & Aly (2012) showed that the kernel functions does affect numerical dissipation in shear flow simulations. The Wendland C4 kernel shows the best conservation properties in their numerical tests. Although MFM solves the fluid equations on the volume elements constructed from the particle distribution, the volume elements themselves are constructed using a specified kernel function hence it is relevant to ask what effect the choice of the kernel function has on the flow solution. Therefore we rerun the MFM-HR-Beta3-TIC simulation with Wendland C4, using 200 neighbours. We found that the simulation still fragments at  $\beta_{crit} = 3$ . This is reassuring as it strengthens the conclusion that the results have truly converged, namely we cannot push  $\beta_{crit}$  even further by reducing numerical dissipation using a more conservative kernel function. However, a word of caution must be said. With such many neighbours the effective gravitational force resolution is half the force resolution in the standard HR simulation, being equal to that in the LR simulations, and the force resolution at later stage is also not directly comparable due to its full adaptive nature.

Meru & Bate (2012) could not prove exact convergence for a set of FARGO simulations, for which they also considered varying the coefficient of viscosity. Indeed, despite showing a trend with resolution that was pointing towards convergence, they did not find  $\beta_{crit}$  to maintain the exact same value when they increased their resolution by a factor of 2. The asymptotic value of  $\beta_{crit}$  suggested by their results was also higher than the corresponding value found in their SPH runs. In light of our findings that show how convergence occurs to a very small value of  $\beta_{crit} = 3$ , we argue that the published FARGO simulations might suffer from even stronger numerical dissipation than SPH, resulting not only from numerical viscosity but also from advection

errors occurring in cuspy regions that are not at all axisymmetric and hence cannot be captured properly by the cylindrical geometry of the grid. For the same reason, significant improvements can be expected using relaxed initial conditions as deviations from axisymmetry are less severe due to the absence of the transition phase. This is once again in line with the findings of (Paardekooper et al. 2011) Advection errors in the interface regions could be even more severe in Cartesian grids, unless aggressive AMR is used to better capture the curvature of the flow. We plan to reassess this in a future comparison employing more than one type of grid-based code.

Finally, at fixed smoothing length the density increase in self-gravitating flow is strongly affected by gravitational softening. Adaptive softening is expected to play a key role as it increases the force resolution as particles converge towards a cusp or sharp interface. We run additional TSPH simulations with fixed softening to quantify the importance of the choice of softening for the problem under study.

Figure 8 indicates that also fixed softening simulations also experience an exponential peak density growth. In the TSPH-LR run, when we choose a gravitational softening of 0.1 code units, which equals half the smoothing length in the disk middle plane at  $r = 9$  (see the curve of the TSPH-LR-Beta4-S0.1 run), the peak volume density evolution is similar to that in the adaptive softening run. If we decrease the softening to 0.05 (TSPH-LR-Beta4-S0.05), the peak volume density increase significantly. The TSPH-LR-Beta4-S0.05 has even higher peak density than TSPH-LR-Beta4-S0.1, and also even higher than the peak density in the adaptive softening run, resulting from the denser cusps forming at higher resolution. As a result, runaway fragmentation in presence of vorticity damping can be even more problematic than in the reference adaptive softening run.

The results found in this paper suggest that disks need to cool really fast to fragment, on a timescale nearly identical to the local orbital time. This reinforces the notion that it is in the outer disk regions, at  $R > 30$  AU (Rafikov 2009; Clarke & Lodato 2009), that the conditions are favourable for fragmentation. However, our study focused on idealized isolated disk models, neglecting the effect of both external triggers, such as mass accretion onto the disk from the envelope in the early stages of disk evolution (Boley & Durisen 2010; Vorobyov & Basu 2010) or internal triggers such as perturbations by a previously-formed fragment (Meru 2015). Mass loading has already been shown to bring disks to fragmentation even when radiative cooling is slow (Boley 2009), or even formally absent as in the col-



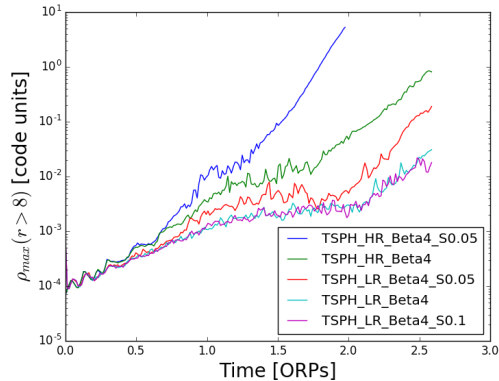


**Figure 8.** The effect of fixed gravitational softening and resolution on peak density inside the interface region at  $r > 8$  during the transition phase. We show the results for a set of TSPH runs, including the reference runs with adaptive softening. The HR simulation with softening 0.02 is stopped early because of small time steps.

lapse of polytropic turbulent cloud cores (Hayfield et al. 2011). The correct treatment of radiative cooling and heating originating from accretion ultimately requires radiative transfer to be employed (eg (Meru & Bate 2011b; Rogers & Wadsley 2011; Mayer et al. 2016) However, attention should be paid to the initial condition setup and accretion boundary condition. Complex flow structures and overdensities arising in turbulent collapse may lead to strong numerical dissipation and cause spurious fragmentation for the same reasons described in this paper. Therefore a weakly dissipative method such as MFM holds promise to be most suitable for radiative disk formation studies as well.

The complexity inherent to model disk fragmentation emerging from our study suggests that it is too premature to use existing simulations to compare with exoplanet detection via imaging surveys for wide orbit gas giants (eg (Vigan et al. 2017)). Indeed, once the formation stage of clumps is robustly modeled, their evolution via further collapse (Galvagni et al. 2012; Szulgyi et al. 2017) and migration in the disk (Baruteau et al. 2011; Malik et al. 2015) is also not completely understood, and not yet firm from the numerical side. Fast inward migration of clumps is routinely found which alone would invalidate any direct comparison with wide orbit gas giants as a way to infer the role of disk instability, but the migration rate in self-gravitating disks might be affected directly or indirectly by numerical dissipation effects. A comparison of hydro methods is warranted in this case as well.

Finally, there is an interesting upshot of our study. This is that actual physical sources of viscosity in disks, such as the magnetorotational instability (MRI) (Balbus

& Hawley 1991) might promote fragmentation if they can dissipate angular momentum efficiently in overdense regions with strong shear. This will be explored in future work.

## 5. CONCLUSIONS

We performed 3D hydrodynamic simulations using SPH with different artificial viscosity implementations as well as with a new Lagrangian method, MFM, which employs a Riemann solver on a volume partition generated by particles, thus not requiring any explicit numerical viscosity.

Our TSPH simulations agree well with a previous study by Meru & Bate (2011a, 2012). They confirm the *non-convergence* of the critical cooling rate for disk fragmentation in a self-gravitating disk. MFM instead attains convergence, and to a significantly lower value of the critical cooling time,  $\beta_{crit} = 3$ . ISPH simulations, which adopt the more conservative artificial viscosity implementation by Cullen & Dehnen (Cullen & Dehnen 2010), resulting formally in no shear viscosity, exhibit an intermediate behaviour. Finally, exact convergence, even in MFN, occurs only with relaxed initial conditions. We find a coherent explanation for our results, showing that the driving effect is numerical dissipation of angular momentum in strong shearing flows. This is exacerbated as resolution is increased, despite shear viscosity in SPH is formally decreasing with resolution, because the flow develops stronger cusps with large velocity derivatives where vorticity is artificially damped. In those regions the characteristic wavelength associated with fragmentation, conservatively measured with the Toomre wavelength, remains poorly resolved even when the number of particles is increased by nearly three orders of magnitude, hence the high sensitivity on the numerical dissipation. Relaxed initial conditions exhibit a more convergent behaviour because they avoid a transient phase in which overdense cusps and associated high velocity derivatives occur, thus suffering less the impact of artificial angular momentum dissipation by numerical viscosity.

We stress that the small value  $\beta_{crit} = 3$  in the converged MFM simulations is significantly smaller than any value previously found in the literature when trying to assess convergence with increasing resolution. This indicates that the trends suggestive of asymptotic convergence reported in the literature for both SPH codes and FARGO (Meru & Bate 2012; Rice et al. 2014) were just reflecting saturation of numerical angular momentum dissipation rather than a decreasing numerical dissipation with increasing resolution.

We have further assessed the validity of our statements by running additional simulations that explore other aspects of SPH implementations, such as adaptive softening, kernel function and form of the hydro force. These tests confirm our claim that only MFM attains exact convergence.

In summary, our results indicate that the use of hydro methods with minimal numerical viscosity is the first necessary step towards predictive simulations of disk instability because the issues we highlighted would still

play a role in complex simulations with radiative transfer and envelope accretion.

We thank Jim Stone, Frederic Masset for useful discussions. We are grateful to Philip Hopkins for helping run the code. Pynbody (Pontzen et al. 2013) is used for the visualization. We acknowledge support from the Swiss National Science Foundation via the NCCR PlanetS. F.M. acknowledges support from The Leverhulme Trust and the Isaac Newton Trust.

## REFERENCES

- Agertz, O., Moore, B., Stadel, J., et al. 2007, *Monthly Notices of the Royal Astronomical Society*, 380, 963
- Backus, I., & Quinn, T. 2016, *MNRAS*, 463, 2480
- Balbus, S. A., & Hawley, J. F. 1991, *ApJ*, 376, 214
- Balsara, D. S. 1995, *Journal of Computational Physics*, 121, 357
- Baruteau, C., Meru, F., & Paardekooper, S.-J. 2011, in *SF2A-2011: Proceedings of the Annual meeting of the French Society of Astronomy and Astrophysics*, ed. G. Alecian, K. Belkacem, R. Samadi, & D. Valls-Gabaud, 459–461
- Bate, M. R. 2011, *MNRAS*, 417, 2036
- Bate, M. R., Bonnell, I. A., & Price, N. M. 1995, *MNRAS*, 277, 362
- Boley, A. C. 2009, *ApJL*, 695, L53
- Boley, A. C., & Durisen, R. H. 2010, *ApJ*, 724, 618
- Boss, A. P., & Bodenheimer, P. 1979, *ApJ*, 234, 289
- Clarke, C. J., & Lodato, G. 2009, *Monthly Notices of the Royal Astronomical Society: Letters*, 398, L6
- Cossins, P., Lodato, G., & Clarke, C. J. 2009, *MNRAS*, 393, 1157
- Cullen, L., & Dehnen, W. 2010, *MNRAS*, 408, 669
- Dehnen, W., & Aly, H. 2012, *MNRAS*, 425, 1068
- Durisen, R. H., Boss, A. P., Mayer, L., et al. 2007, *Protostars and Planets V*, 607
- Galvagni, M., Hayfield, T., Boley, A., et al. 2012, *MNRAS*, 427, 1725
- Gammie, C. F. 2001, *ApJ*, 553, 174
- Hawley, J. F., Gammie, C. F., & Balbus, S. A. 1995, *ApJ*, 440, 742
- Hayfield, T., Mayer, L., Wadsley, J., & Boley, A. C. 2011, *MNRAS*, 417, 1839
- Helled, R., Bodenheimer, P., Podolak, M., et al. 2014, *Protostars and Planets VI*, 643
- Hernquist, L., & Katz, N. 1989, *ApJS*, 70, 419
- Hopkins, P. F. 2013, *Mon. Not. R. Astron. Soc.*, 428, 2840
- . 2015, *MNRAS*, 450, 53
- Hu, C. Y., Naab, T., Walch, S., Moster, B. P., & Oser, L. 2014, *MNRAS*, 443, 1173
- Kaufmann, T., Mayer, L., Wadsley, J., Stadel, J., & Moore, B. 2007, *MNRAS*, 375, 53
- Keller, B. W., Wadsley, J., Benincasa, S. M., & Couchman, H. M. P. 2014, *MNRAS*, 442, 3013
- Klee, J., Illenseer, T. F., Jung, M., & Duschl, W. J. 2017, *ArXiv e-prints*, arXiv:1704.02193
- Malik, M., Meru, F., Mayer, L., & Meyer, M. 2015, *ApJ*, 802, 56
- Mayer, L., & Gawryszczak, A. J. 2008, in *Astronomical Society of the Pacific Conference Series*, Vol. 398, *Extreme Solar Systems*, ed. D. Fischer, F. A. Rasio, S. E. Thorsett, & A. Wolszczan, 243
- Mayer, L., Peters, T., Pineda, J. E., Wadsley, J., & Rogers, P. 2016, *ApJL*, 823, L36
- Mayer, L., Quinn, T. R., Wadsley, J., & Stadel, J. 2004, in *Bulletin of the American Astronomical Society*, Vol. 36, *AAS/Division of Dynamical Astronomy Meeting #35*, 851
- Mayer, L., Wadsley, J., Quinn, T., & Stadel, J. 2005, *MNRAS*, 363, 641
- Meru, F. 2015, *MNRAS*, 454, 2529
- Meru, F., & Bate, M. R. 2011a, *MNRAS*, 411, L1
- . 2011b, *MNRAS*, 410, 559
- . 2012, *MNRAS*, 427, 2022
- Monaghan, J. J., & Gingold, R. A. 1983, *Journal of Computational Physics*, 52, 374
- Morris, J., & Monaghan, J. 1997, *Journal of Computational Physics*, 136, 41
- Nelson, A. F. 2006, *MNRAS*, 373, 1039
- Ormel, C. W., Kuiper, R., & Shi, J.-M. 2015a, *MNRAS*, 446, 1026
- Ormel, C. W., Shi, J.-M., & Kuiper, R. 2015b, *MNRAS*, 447, 3512
- Paardekooper, S. J. 2012, *MNRAS*, 421, 3286

- Paardekooper, S.-J., Baruteau, C., & Meru, F. 2011, MNRAS, 416, L65
- Pickett, B. K., Mejia, A. C., & Durisen, R. H. 2001, in Bulletin of the American Astronomical Society, Vol. 33, American Astronomical Society Meeting Abstracts, 1397
- Pontzen, A., Roškar, R., Stinson, G. S., et al. 2013, pynbody: Astrophysics Simulation Analysis for Python, , astrophysics Source Code Library, ascl:1305.002
- Price, D. J. 2008, Journal of Computational Physics, 227, 10040
- Price, D. J., & Monaghan, J. J. 2007, MNRAS, 374, 1347
- Rafikov, R. R. 2009, ApJ, 704, 281
- Read, J. I., Hayfield, T., & Agertz, O. 2010, MNRAS, 405, 1513
- Rice, W. K. M., Lodato, G., & Armitage, P. J. 2005, MNRAS, 364, 56
- Rice, W. K. M., Paardekooper, S.-J., Forgan, D. H., & Armitage, P. J. 2014, MNRAS, 438, 1593
- Rogers, P. D., & Wadsley, J. 2011, MNRAS, 414, 913
- Rosswog, S., Davies, M. B., Thielemann, F.-K., & Piran, T. 2000, A&A, 360, 171
- Shen, S., Wadsley, J., Hayfield, T., & Ellens, N. 2010, Monthly Notices of the Royal Astronomical Society, 401, 727
- Springel, V. 2005, MNRAS, 364, 1105
- Szulgyi, J., Mayer, L., & Quinn, T. 2017, Monthly Notices of the Royal Astronomical Society, 464, 3158
- Tamburello, V., Mayer, L., Shen, S., & Wadsley, J. 2015, MNRAS, 453, 2490
- Toomre, A. 1964, ApJ, 139, 1217
- Vigan, A., Bonavita, M., Biller, B., et al. 2017, ArXiv e-prints, arXiv:1703.05322
- Vorobyov, E. I., & Basu, S. 2010, ApJ, 719, 1896
- Young, M. D., & Clarke, C. J. 2015, MNRAS, 451, 3987

## APPENDIX

## A. ISOTHERMAL SPHERE COLLAPSE

To further assess the low numerical viscosity in MFM we run the standard isothermal test case for the collapse of a rotating molecular cloud. This test, first described by [Boss & Bodenheimer \(1979\)](#), is a typical test case for numerical codes studying fragmentation ([Bate et al. 1995](#)). An initially isothermal, spherical, self-gravitating hydrogen molecular cloud starts to collapse from rest. Physical viscosity and the magnetic field are not included, so the angular momentum of the system should be conserved. The gas is assumed to be ideal gas and initial temperature is  $10K$ . The mass of the cloud is  $1M_{sun}$ , and radius of the cloud is  $3.2 \times 10^{16}cm$ . The angular velocity is  $\Omega = 1.6 \times 10^{-12}rads^{-1}$ . The ratios of thermal energy to the magnitude of gravitational energy, and rotational energy to the magnitude of gravitational energy of  $\alpha = 0.25$  and  $\beta = 0.20$ , respectively. The mean density is  $\rho = 1.44 \times 10^{-17}gcm^{-3}$ . No density perturbation is imposed initially. The free-fall time for the initial cloud is  $t_{ff} = 5.52 \times 10^{11}s$ .

We run this setup with 10K, 100K, 1M particles, using both MFM and TSPH. All the simulations share the same properties discussed below. In figure 9, we plot the specific angular momentum profile of the sphere at different times.

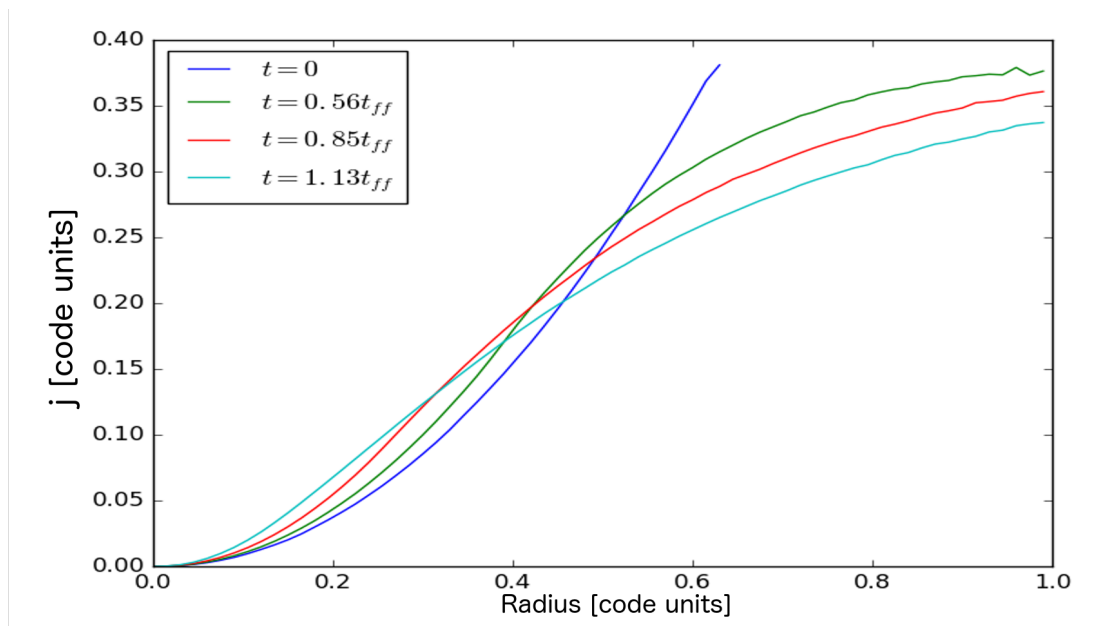


**Figure 9.** The evolution of the specific angular momentum profile in the MFM collapsing rotating isothermal sphere run with 1M particles

Initially the sphere is uniformly rotating, and the special angular momentum  $j \propto r^2$ , where  $r$  is the radius. The initial cloud radius is about 0.6 code length units. When material starts to flow inwards, angular momentum must be transported outward in order to conserve the total angular momentum of the system. Particles at the outer part of the cloud drift further. We show the angular momentum profile out to only one code length unit because the outer part is noisy due to low number of particles.

The angular momentum profile evolves less at higher resolution in 11, which is a sign of less numerical dissipation. This is because of the nice continuous flow property and numerical viscosity scales with  $h$ . From figure 10, we see very similar evolution of angular momentum profile by MFM and TSPH. However, at fixed time, the TSPH angular momentum profile (dashed lines) has evolved a bit faster, ie, more angular momentum has been transported outwards, which is reflected by the fact that the MFM curve is above the TSPH curve inside 0.6 code length units and below outside.

We caution that the changing nature of the flow with increasing resolution, which we have shown to be a central aspect of unstable disk evolution, does not play a role here. This also means there are no sites of strong shear and



correspondingly strong numerical dissipation as in the disk simulations. Therefore the fact that MFM appears to perform only marginally better than TSPH is not surprising as this is an easy flow configuration to handle.

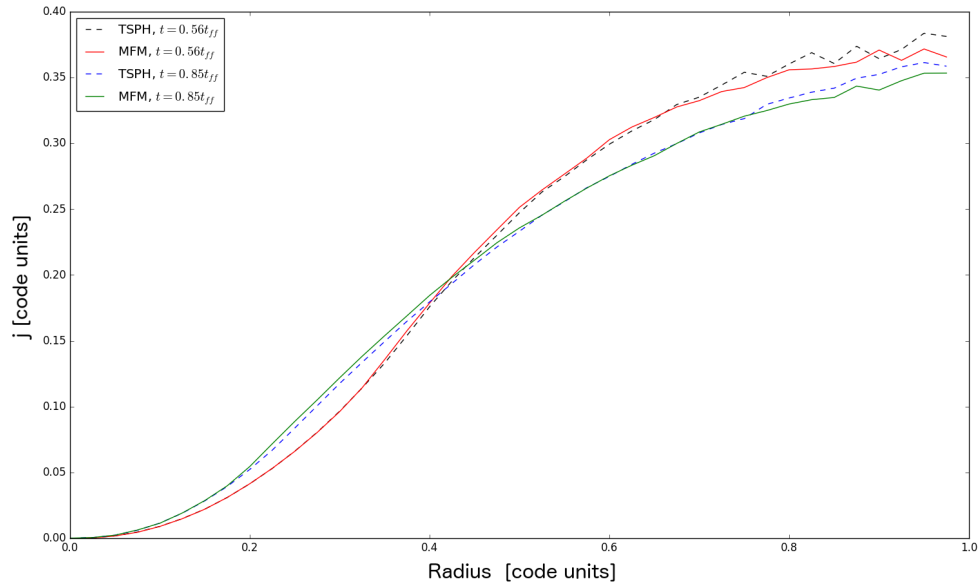


**Figure 10.** Specific angular momentum profile with both MFM and TSPH, using 100K particles. At fixed time, the angular momentum profile evolves slightly faster in TSPH due to more significant numerical transport.

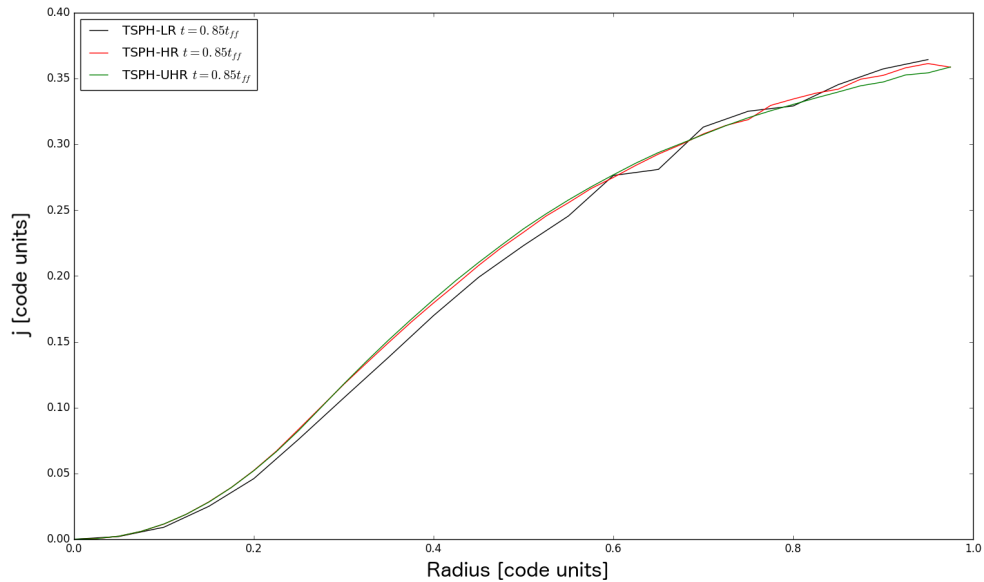


**Figure 11.** Resolution dependence of the angular momentum profile in TSPH runs, using 10K (LR), 100K (HR) and 1 M particles (UHR)

## B. ACCRETING PLANET TEST

We are interested in assessing how numerical viscosity affects the angular momentum transport, especially in cusps at interface regions where high velocity derivatives occur. . To avoid the complexity of resolving a full disk but carry out a test that can address a configuration with velocity derivatives, we use a 2D shearing sheet (Hawley et al. 1995) with an active accreting planet in the center to mimic the collapse under self-gravity. The simulations are similar to those in Ormel et al. (2015a) while the gravity of the planet is added following Ormel et al. (2015b). We choose the local sound speed and the disk scale height as the natural units of speed and length, respectively. We set the gravitational constant to 1. The planets dimensionless mass  $m \equiv GM_p/(c_s^3/\Omega)$  equals its Bondi radius in dimensionless units  $R_{Bondi}/H$ . In these units the dimensionless Hill sphere  $r_{Hill} = R_{Hill}/H = (m/3)^{1/3}$ .

The gravity of the planet is added  $F(t) = F_0\{1 - \exp[-\frac{1}{2}(\frac{t}{t_{inj}})^2]\}$ . The force increases gradually to mimic the collapse due to self-gravity.  $t_{inj}$  is the injection time. The gravity from the planet is smoothed to avoid numerical instability and increase the efficiency of calculation.  $F_0 = -\frac{m}{r^2}\exp[-A(\frac{r_{in}}{r})^p - B(\frac{r}{r_{out}})^q]$ . We set A=10, p=8 and B=1, q=4. The force transits from a pure Newtonian force  $F_0 = -m/r^2$  for  $r_{in} < r < r_{out}$  to zero continuously and quickly. We set  $r_{in} = 0.1, r_{out} = m$  to prevent boundary condition corruption by the gravity of the planet.

We run simulations with  $m = 0.2, t_{inj} = 2$  at a resolution of  $64 \times 64$  particles (this means 64 particles per scale height, which is even higher resolution than the 16 million particles UHR 3D disk runs used in this paper). The artificial viscosity  $\alpha$  coefficient is shown in figure12 to compare directly TSPH and ISPH. ISPH, as expected, has lower artificial viscosity. We use the time evolution of peak density to measure how much mass is accreted over time inside the planet radius  $r_{in}$  as shown in figure 13. The faster the growth of peak density the faster must be the outward transport of angular momentum resulting from any form of numerical dissipation, including, but not only, explicit artificial viscosity. Figure 13 highlights the lower dissipation of MFM. Indeed MFM always has the lowest peak density while ISPH and TSPH are almost identical despite the lower value of the  $\alpha$  coefficient. We argue the faster accretion in SPH methods is due to higher numerical viscous dissipation. The Cullen & Dehnen switch is most effective away from shocks and it is not able to effectively suppress numerical viscosity in a flow with a large velocity gradient as in this test.

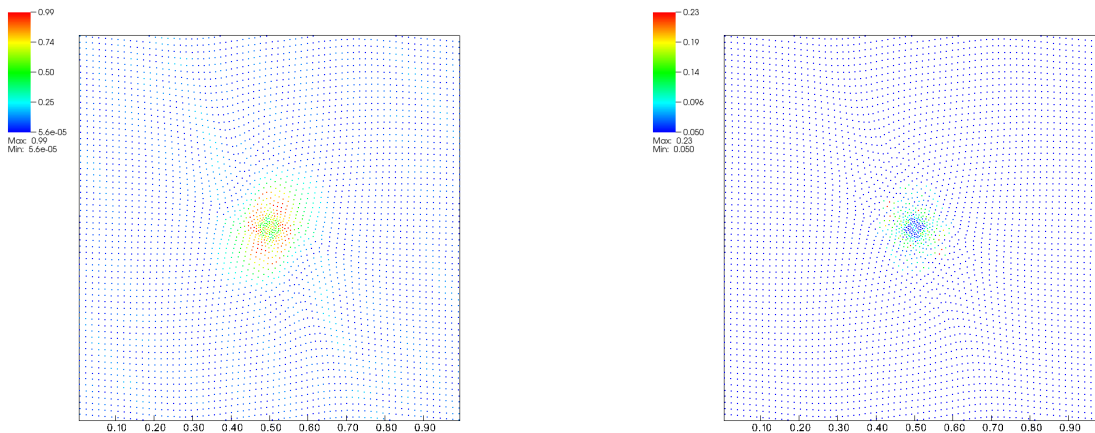


**Figure 12.** Artificial viscosity  $\alpha$  coefficient in TSPH (left) and ISPH accreting sink test (right) at  $t = 2$ . ISPH has smaller artificial viscosity coefficient around the accretion flow due to the Cullen and Dehnen switch.

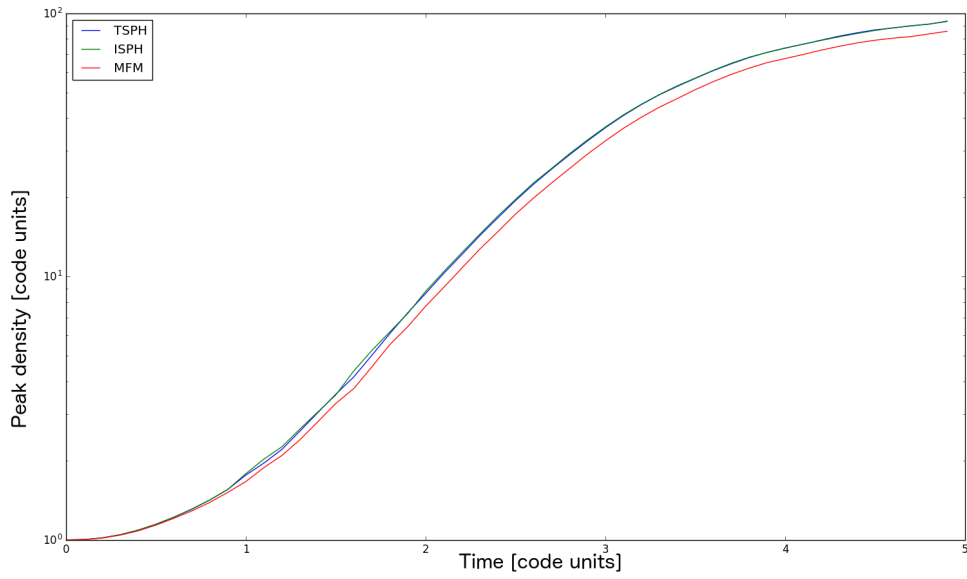


**Figure 13.** The peak volume density evolution with SPH and MFM. MFM always has the highest peak density, reflecting a lower accretion rate.